Six image phase stepped photoelasticity for the quantification of the stress field around 25 μm reinforcing fibres

Z. Liu, F.M. Zhao, F.R. Jones

▶ **To cite this version:**

Z. Liu, F.M. Zhao, F.R. Jones. Six image phase stepped photoelasticity for the quantification of the stress field around 25 μm reinforcing fibres. Composites Science and Technology, 2010, 70 (14), pp.2039. 10.1016/j.compscitech.2010.07.011 . hal-00682263

HAL Id: hal-00682263
https://hal.science/hal-00682263

Submitted on 24 Mar 2012

HAL is a multi-disciplinary open access archive for the deposit and dissemination of scientific research documents, whether they are published or not. The documents may come from teaching and research institutions in France or abroad, or from public or private research centers.

L'archive ouverte pluridisciplinaire **HAL**, est destinée au dépôt et à la diffusion de documents scientifiques de niveau recherche, publiés ou non, émanant des établissements d'enseignement et de recherche français ou étrangers, des laboratoires publics ou privés.

Accepted Manuscript

Six image phase stepped photoelasticity for the quantification of the stress field around 25 μm reinforcing fibres

Z. Liu, F.M. Zhao, F.R. Jones

PII: S0266-3538(10)00268-X
DOI: 10.1016/j.compscitech.2010.07.011
Reference: CSTE 4765

To appear in: *Composites Science and Technology*

Received Date: 9 April 2010
Revised Date: 5 July 2010
Accepted Date: 10 July 2010

Please cite this article as: Liu, Z., Zhao, F.M., Jones, F.R., Six image phase stepped photoelasticity for the quantification of the stress field around 25 μm reinforcing fibres, *Composites Science and Technology* (2010), doi: 10.1016/j.compscitech.2010.07.011

This is a PDF file of an unedited manuscript that has been accepted for publication. As a service to our customers we are providing this early version of the manuscript. The manuscript will undergo copyediting, typesetting, and review of the resulting proof before it is published in its final form. Please note that during the production process errors may be discovered which could affect the content, and all legal disclaimers that apply to the journal pertain.

ACCEPTED MANUSCRIPT

Manuscript draft for Composites Science and Technology

Title: Six image phase stepped photoelasticity for the quantification of the stress field around 25 μm reinforcing fibres

Corresponding Author: Prof. F.R. Jones

Corresponding Author's address:

The University of Sheffield, Mappin Street, Sheffield S1 3JD, UK

Tele: +44 (0) 114 222 5477

Fax: +44 (0) 114 222 5943

Email: f.r.jones@sheffield.ac.uk

First Author: Zheng Liu, PhD

Order of Authors: Zheng Liu, Fangming Zhao, Frank R. Jones

Abstract:

A six image phase stepped photoelastic technique has been applied for the measurement of the interfacial shear stress distribution in the matrix resin along a reinforcing E-glass fibre of ~ 25 μm at its end and at a fibre-break. Contour maps of the isochromatic fringe order and its corresponding isoclinic angle, which are related to the principal stress difference and direction relative to the fibre axis, could be obtained continuously using this photoelastic technique. Thus the actual interfacial shear stress along the fibre can be

ACCEPTED MANUSCRIPT

calculated. Furthermore in the presence of a fibre-break, interfacial debonding and matrix yielding during stress transfer was investigated.

Keywords:

B. Debonding; B. Fracture; B. Interfacial strength; C. Stress transfer; Photoelasticity

ACCEPTED MANUSCRIPT

ACCEPTED MANUSCRIPT

Six image phase stepped photoelasticity for the quantification of the stress field around 25 µm reinforcing fibres

Z. Liu, F.M. Zhao[1], F.R. Jones*

Ceramics and Composites Laboratory, Department of Engineering Materials,

The University of Sheffield, Mappin Street, S1 3DJ, UK

[1] International Paint Ltd., Stoneygate Lane, Felling Gateshead,

Tyne & Wear, NE10 0JY, UK.

* Tele: +44 (0) 114 222 5477 Fax: +44 (0) 114 222 5943

Email: f.r.jones@sheffield.ac.uk

Abstract

A six image phase stepped photoelastic technique has been applied for the measurement of the interfacial shear stress distribution in the matrix resin along a reinforcing E-glass fibre of ~ 25 µm at its end and at a fibre-break. Contour maps of the isochromatic fringe order and its corresponding isoclinic angle, which are related to the principal stress difference and direction relative to the fibre axis, could be obtained continuously using this photoelastic technique. Thus the actual interfacial shear stress along the fibre can be calculated. Furthermore in the presence of a fibre-break, interfacial debonding and matrix yielding during stress transfer was investigated.

Keywords: B. Debonding; B. Fracture; B. Interfacial strength; C. Stress transfer; Photoelasticity

1. Introduction

ACCEPTED MANUSCRIPT

The photoelastic method has been used for analysis of interfacial stresses in fibre composites. Schuster and Scala [1] reported on its application to sapphire whiskers in a birefringent resin. More recently, Fiedler and Schulte [2] applied this technique to glass fibres in a resin. In recent studies, Zhao et al. [3 - 8] have applied the 4 image phase stepping automated photoelastic technique of Patterson and Wang [9] to single embedded fibres. This technique can provide full field maps of the relative retardation and the isoclinic angle. By the application of an unwrapping algorithm [10], a continuous map of isochromatic fringe order can be obtained. It has been used to investigate the stress field in a matrix and the stress distribution at the interface in model composites [5, 6, 9]. In the previous studies, the photoelastic technique has been limited to relatively large diameter fibres of > 80 μm because of the loss of light intensity through the optics and the high stress fringe constant of the matrix resins. Patterson and Wang [11] have developed a four image phase-stepping automated photoelastic camera for the simultaneous observation and recording of the four images required to solve the equations for quantification. Zhao and Jones [3, 5-7] succeeded in applying this technique to investigate the interfacial shear stresses in model single fibre composites. Full profiles of the interfacial shear stress could be determined by assuming that the principle stress at the interface is one of shear. Thus the initiation and propagation of interfacial debonds at fibre-breaks and matrix cracks have been studied. The technique records the principle stress difference $(\sigma_1 - \sigma_2)$ so that within the matrix full quantification is not possible, however Zhao et al. [3] were able to observe trends in the radial direction from fibre which showed that interfacial bond formation was a curing temperature dependent. For a fibre of a few micrometers in diameter, a smaller region of the matrix at the interface is perturbed so that a higher resolution microscope and increased light transmission are needed. However in the 4 image phase stepped system,

ACCEPTED MANUSCRIPT

the polarized light is divided into four beams by Cubic beam splitters, at which losses in light intensity are significant, which leads to difficulties in processing the image by the multiplex software [3, 11]. This limits the application of four image phase-stepping photoelasticity to relatively low magnifications where the signal remains intense.

In this present work, a six image phase-stepping photoelastic technique has been developed to investigate the interfacial shear stress at the surface of fibres of smaller diameter: In this case a glass fibre of 25 μm in an epoxy resin. Each of 6 images can be acquired directly using an elliptically polarized light beam by a digital camera without the need for the cubic beam splitters, to achieve a high quality images of 720×720 μm^2 in size for photoelastic analysis .

2. Experimental

Unsized and unsilanised E-glass fibres used in this study were provided by Owens Corning (Battice,Belgium) with the diameter of 25 ± 1.2 μm, during manufacture, only water was used to cool the fibres.

The matrix resin used in this study was a mixture of Araldite LY 5052 epoxy resin, and 38 phr (parts per hundred resin by weight) Aradur HY 5052 hardener, produced by Huntsman (UK), which were supplied by Advanced Composites Group (UK). The resin blend was cured at room temperature for at least 7 days. The room-temperature cured epoxy resin was chosen in order to avoid the induction of a residual thermal stress on cooling from a curing temperature [7, 8]. The properties of the fibre and cured resin are shown in Table 1.

ACCEPTED MANUSCRIPT

The stress-fringe constant, f_σ, was determined in a tensile test on the epoxy resin casting. Under monochromatic polarised light the specimen was either completely dark or bright (i.e. fringe order N = 0, 0.5, 1, 1.5 …) as the applied stress was increased, as shown in equation 1.

$$f_\sigma = \frac{(\sigma_1 - \sigma_2)t}{N} \qquad (1)$$

where t is the thickness of the specimen, $(\sigma_1 - \sigma_2)$ is the principal stress difference, f_σ is the stress-fringe constant of the resin, i.e. the slope of the curve of $(\sigma_1 - \sigma_2)\,t$ against fringe order N, which is 20.23 MPa/fringe/mm in the elastic range of the resin (Table 1), the same as that measured by Zhao et al [3].

3. Six image phase-stepping photoelastic technique

A phase-stepping automated polariscope was combined with a horizontal tensile mini-tester with a 2 kN load cell and microscope during fragmentation for the measurement of the stress field in an epoxy resin around fibre-breaks. The principle of the instrument is shown in Figure 1. It is equipped with a digital camera (Panasonic WV-BP330) for collecting six photoelastic images by rotating the positions (α, β) of a quarter wave plate (Q_2) and the analyser (A). The relative position of Q_2 and A are given in Table 2, thus generating six different phase-stepped images. Table 2 also shows the position of the other optical elements, the polariser and the quarter wave plate (Q_1), which were kept at 0^0 and -45^0. A monochromatic light made up from deep yellow wavelength at 589.3 ± 0.3 nm was used. The light is elliptically polarised, and then passes through the specimen, which is subjected to a tensile load, quarter-wave plate and analysers, and is focused by objective lenses, on to the digital camera. By rotating the angles of the Q_2

ACCEPTED MANUSCRIPT

quarter wave plate and the analyser, the six images can be obtained, which can be processed by a multiplexer to combine them into a single composite image that can be digitized by a single frame-grabber.

The automated polariscope allowed continuous monitoring of the stress build-up at fibre-breaks and fibre-ends, which enable the load transfer at the interface to be stimulated. The magnitude and direction of stresses at any point can be determined by examination of the fringe pattern, *i.e*. isochromatic and isoclinic fringes. Photoelastic analysis does not require the necessary saturation in fibre fragmentation to be reached [3, 11]. The polariscope uses the method of phase-stepping to determine the relative retardation and isoclinic angles. Table 2 shows the rotating angles of analyzer and Q_2 quarter-wave plate to capture six images. When the analyzer and its associated quarter-wave plate are set to produce circularly polarised light, the intensity of light emitted from a polariscope can be described by the following equation [9],

$$i_n = i_m + i_v\{\sin 2(\alpha-\theta)\cos\delta - \sin 2(\theta-\beta)\cos 2(\alpha-\beta)\sin\delta\} \qquad (2)$$

where n = 1, 2, …6, β and α are the angular orientations of the analyser and its associated quarter-wave plate, respectively, with respect to the polariser. θ and δ are the isoclinic angle and the relative retardation, respectively. The isoclinic fringe pattern represents the contours of equal angles between the direction of the highest principal stress, σ_1, and the fibre axis. It depends only on the angle between the specimen or fibre axis and the optical set-up. i_m and i_v are the intensities of stray light observed when all the optical axes of all the elements and the specimen are parallel. The unknown isoclinic angle and relative retardation are found from six light intensities, i_1, i_2, … i_6 measured for each point (x, y) at different values of β and α, and using following equations:

ACCEPTED MANUSCRIPT

$$\theta = \frac{1}{2}\tan^{-1}\left(\frac{i_5 - i_3}{i_4 - i_6}\right) \tag{3}$$

$$\delta = \tan^{-1}\left(\frac{i_4 - i_6}{(i_1 - i_2)\cos 2\theta}\right) \tag{4}$$

The automated system supplied by Wang's DTS Ltd. (UK) [9] possesses unwrapping algorithms which are used to produce a continuous map of relative retardation. The map of relative retardation can be converted to isochromatic fringe order by a software operation [9]. The isochromatics only depend on the applied stress, which have nothing to do with the fibre centre axis and the optical set-up. The relative retardation, δ, in the specimen is related to the fringe order, *N*, [12], as follows:

$$\delta = 2\pi N \tag{5}$$

In photoelasticity, the relationship of the isochromatic fringe order, *N*, the principal stresses σ_1 and σ_2, and maximum shear stress, τ_{max} in a two dimensional model as described by the following equation:

$$\tau_{\max} = \frac{1}{2}(\sigma_1 - \sigma_2) = \frac{f_\sigma N}{2t} \tag{6}$$

where t is the thickness of the specimen. In fact, the stresses are not constant through the thickness of a resin matrix specimen containing a high Young's modulus fibre, and the observed values of the principal stress difference or maximum shear stress are an average. To correct for the depth of the resin at the interface, equation 7 is used [1, 2]. The corrected maximum shear stress, τ_{cmax}, can be calculated by the following equation [1],

$$\tau_{c\max} = 0.5\left(\frac{t(\sigma_0 - \sigma_n)(r_1 - r_0)}{2\left\{r_1 a - 0.5\left[r_1 a + (r_0 + y)^2 \log\left(\frac{a + r_1}{r_0 + y}\right)\right]\right\}} + \sigma_n\right) \tag{7}$$

ACCEPTED MANUSCRIPT

Where $a = \sqrt{r_1^2 - (r_0 + y)^2}$, σ_0 is the observed principal stress difference at the interface. σ_n is normal applied matrix stress. The other variables are defined in Figure 2. r_0 is the fibre radius. r_1 is the distance from centre of fibre to the point where the radial distribution of applied matrix stress falls to zero. y is the distance from edge of fibre, y = 0 at the interface. z is a dummy variable, defined by $z = r_1\cos\theta$ at $r = r_1$, $z = 0$ at $r = r_0 + y$. t is thickness of the specimen.

The actual interfacial shear stress τ_i between the fibre and matrix resin can be calculated from the corrected maximum shear stress, τ_{cmax}, and the isoclinic angle, θ, according to Mohr's circle [2].

$$\tau_i = \tau_{cmax}\sin 2\theta \qquad (8)$$

4. Results

4.1 Stress near a fibre-end

Figures 3-5 show the contour maps of fringe order in the matrix resin around a 15.1 mm long E-glass fibre-end at the applied matrix stresses of 18.38, 25.61 and 32.53 MPa. The dimensions of the matrix region in the contour map of fringe order are 0.51 mm by 0.31 mm. It can be seen that there are regions of high fringe order in the vicinity of the fibre, indicating the existence of a high stress concentration zone. At an applied stress of 18.38 MPa in Figure 3, the stress concentration region appeared at the rim of the fibre-end and at a short distance along the fibre. On increasing applied load to 25.61 MPa, the region of high fringe order extended along the fibre. The maximum fringe order occurred in the matrix near the interface. As the applied load was further increased to

ACCEPTED MANUSCRIPT

32.53 MPa, the region of high fringe order propagated along the fibre, away from the fibre-end. This indicated that a debond had been initiated.

These images can be quantified by applying the analysis described in equations 3 - 8. At the fibre-matrix interface, a shear stress dominates so that the interfacial shear stress can be calculated from the principal stress difference at the interface. Figure 6 shows the profiles of interfacial shear stress for the 25 μm fibre in the epoxy resin at the three different applied stresses. It can be seen that on increasing the applied load, the maximum interfacial shear stresses increased. At an applied stress of 18.38 MPa, the maximum value of interfacial shear stress is very close to fibre end, however on increasing the applied load, the maximum value moved along the fibre. Since the maximum can be associated with the bonded interface we can see that at a high load, a debond forms and propagates along the fibre. The shear stress decays according to that of a well bonded fibre [6]. The peaks in the shear stress curves in the bonded region occurred at ~ 7, 18 and 33 μm away from the fibre-ends at the loads of 18.38, 25.61 and 32.53 MPa, respectively, which correspond to the maximum interfacial shear stresses: 26.87, 30.22 and 33.20 MPa. The maximum interfacial shear stresses at the applied stresses of 25.61 and 32.53 MPa, are higher than the matrix shear yielding stress of 27.7 ± 1.4 MPa (Table 1), so that the debond happened at the fibre-end. Therefore, the interfacial bond shear strength could have a value between 26.87 and 30.22 MPa.

4.2 Stresses near a fibre-break

Figures 7 shows the contours of the fringe order at the first fibre-break at an applied stress of 24.69 MPa. The area examined has the dimensions of 0.64 mm by 0.50 mm. The left fragment associated with the break is 4.65 mm long, the right fragment is 4.71

ACCEPTED MANUSCRIPT

mm in length. From Figure 7 it can be seen that the highest fringe order appears at the end of the fibre-break and extends along the interface with the fibre. On increasing the applied stress to 33.09 MPa, the interfacial shear stress exhibited a symmetrical distribution at the fibre-break. The region of high fringe order propagated along the fibre away from the fibre-break (Figure 8). In order to simplify the calculation of the interfacial shear stress, the only top right areas in Figures 7 and 8 were quantitatively analyzed. The interfacial shear stress profile was calculated from the fringe order directly at the interface along the fibre from the end of the fibre-break (Figure 9). With the reloading of fibre after fracture, a high region of fringe order appeared at the interface near the fibre-break at an applied stress of 24.69 MPa. The maximum interfacial shear stress of 30 MPa was observed to occur at ~ 13 μm away from the fibre-break. There was no evidence of a debond in the optical micrograph at this axial load. Therefore yielding of the interphasal matrix appears to have arisen from the resolved shear stress reaching 30 MPa. Compared with the above analysis, the interfacial bond shear strength could be ~ 30 MPa. At the higher applied stress of 33.09 MPa, the interfacial shear stress reached a maximum of 36.3 MPa at a distance of 39 μm away from the fibre-break. The minimum in the shear stress profile is at 12 μm in Figure 9, which corresponded to the observed interfacial debonding length, recorded in the optical micrograph shown in Figure 10.

5. Discussion

In this work, 6 image phase stepped photoelasticity was introduced to successfully measure the stress field around 25 μm diameter fibres. By increasing the resolution of microscope and light transmission, the change in fringe order in the small region of 720 × 720 μm^2 at the interface was clearly recorded. This enabled the variation in interfacial

ACCEPTED MANUSCRIPT

shear stress with applied load to be studied. Using this technique, real-time data could be obtained for the strain field in the matrix resin at the fibre-end and fibre-break for a fibre about 20 microns in diameter, which is of typical dimensions of an industrial reinforcement. This therefore, has an advantage over common micro-mechanical techniques, such as fibre fragmentation or pull-out for investigating the interfacial properties because the data analysis does not require the assumptions associated with the theoretical models employed. The micro-mechanisms of stress transfer in fibre composites can be observed by this technique. The main disadvantages are associated with the intensity of the transmitted light under high magnification. The similarity of the matrix stress profiles at fibre-breaks and fibre-ends obtained by photoelasticity with those from embedded carbon nanotubes-Raman sensors demonstrates the advantage of mapping the strain in the interfacial matrix of model fibre-matrix composites [13-16].

Fibre fracture, interfacial debonding and propagation, and interfacial yielding are all involved in the micromechanics of the fracture of a fibre composite. These have been shown to significantly influence the matrix stress field and hence the magnitude of the interfacial shear stress which results from stress transfer into the unbroken fragments [3, 6]. In this study, interfacial debonding was found to be initiated after matrix yielding and propagate along the fibre from the fibre-end, during fragmentation despite the lack of a fibre-surface treatment. However at a free fibre-end, the maximum shear stress was shown to move away from the fibre-end on increasing the axial load (Figure 6). This was an indication of debonding which resulted from the stress concentration at the free-end. With the applied stress increasing, the frictional shear stress at the debonded interface has a range of values, because of the complex micromechanics of failure, involving partial and complete debonding [4].

ACCEPTED MANUSCRIPT

At a fragment-break, debonding did not occur immediately under an axial stress of 24.69 MPa. However shear yielding of the matrix in the vicinity of the fibre/matrix interface was observed to proceed debonding which occurred at the higher applied stress of 33.09 MPa, as shown in Figure 9.The stress transfer profile at an applied stress of 24.69 MPa did not exhibit features typical of debonding but showed a constant shear stress indicative of interphasal matrix yield. However on increasing the applied stress from 24.69 to 33.09 MPa, interfacial debonding at the fibre/matrix interface clearly occurred. The minimum in the interfacial shear stress profile was shown to correspond to a debonded region as shown in Figure 10.

The most significant result from this study is the differing interfacial response to stress transfer at a free fibre-end and at fibre-break. The fibre used had not had a silane or other surface treatment. Furthermore the resin was cured at room temperature over a long period of 7 days. Residual stresses in the sample can be considered to be negligible, since relaxation of cure shrinkage stresses can be anticipated during the long-term sample preparation. Firstly the long-considered adhesion of bare glass to epoxy resin is demonstrated. However, debonding could be initiated at a free-end by the stress concentration associated with the free edge. However during fragmentation the stored energy which is released leads to matrix yield which dissipates the energy. Debonding in this case only occurs when the interfacial shear bond strength is exceeded. This observation may explain some discrepancies from calculating bond strengths from the average fragment length. An interfacial bond strength was found to be ~ 30 MPa which is close to the matrix yield strength of 27.7 ± 1.4 MPa, explaining the complex

ACCEPTED MANUSCRIPT

micromechanics. 6-phase stepped photoelasticity has also proved successful in identifying these micromechanics.

6. Conclusions

A six image phase-stepping photoelastic analysis is a feasible method for the quantitative determination of stress distributions in fine diameter single fibre composites. It can be directly applied to an investigation of the in-situ matrix stress or interfacial shear stress distributions in low diameter fibre / epoxy system. The six image phase-stepping photoelasticity is able to quantify the propagation of interfacial debonding, as well as identify delays associated with matrix yielding. This technique allows a full study of interfacial micromechanics in model fibre composites. This study has shown that bonding of unsilanised glass fibre to epoxy resin occurs and that a mixed micromechanics of interphasal yield and debonding occur at fibre-ends and fragments.

Acknowledgements

This work was supported by an EPSRC portfolio grant. The authors gratefully acknowledge Vantico Ltd for the supply of resins and Owen Corning Ltd for the supply of E-glass fibres.

References

1. Schuster DM and Scala E. The Mechanical interaction of sapphire whiskers with a birefringent matrix. Transactions of the Metallurgical Society of AIME, 1964, 230, 1635 – 1640.

2. Fiedler B and Schulte K. Photo-elastic analysis of fibre-reinforced model composite materials. Compos. Sci Tech, 1997, 54, 859 – 867.

ACCEPTED MANUSCRIPT

3. Zhao FM, Hayes SA, Patterson AE, Young RJ, Jones FR. Measurement of micro stress fields in epoxy matrix around a fibre using phase-stepping automated photoelasticity. Compos. Sci. Tech, 2003, 63, 1783 – 1787.

4. Zhao FM, Martin RDS, Hayes SA, Patterson EA, Young RJ, Jones FR. Photoelastic analysis of matrix stresses around a high modulus sapphire fibre by means of phase-stepping automated polariscope. Composites Part A, 2004, 1 – 16.

5. Zhao FM, Hayes SA, Patterson AE, Young RJ, Jones FR. Photoelastic analysis of matrix stresses around a glass fibre in fragmentation test by means of phase-stepping automated polariscope. Composites Part A, 2005, 36, 229 – 224.

6. Zhao FM, Patterson AE, Jones FR. Phase-stepping photoelasticity for quantifying the interfacial response in fibre composites at fibre-breaks. Mater Sci Eng A, 2005, 412, 83 – 87.

7. Zhao FM, Hayes SA, Patterson AE, Jones FR. Phase-stepping photoelasticity for the measurement of interfacial shear stress in single fibre composites. Composites Part A, 2006, 37, 216 – 221.

8. Zhao FM and Jones FR. Thermal loading of short fibre composites and the induction of residual shear stresses. Composite Part A, 2007, 38 (11), 2374 – 2381.

9. Patterson EA and Wang ZF. Towards full field automated photoelastic analysis of complex components. Strain, 1991, 27 (2), 49 – 56.

10. Wang ZF and Patterson EA. Use of phase stepping with demodulation and fuzzy sets for birefringence measurement. Optics and Lasers in Engineering, 1995, 22, 91-104.

11. Patterson EA and Wang ZF. Simultaneous observation of phase-stepped images for automated photoelasticity. J Strain Analysis, 1998, 33, 1 – 15.

12. Dally JW and Riley WF. Experimental stress analysis. New York: McGraw-Hill, 1985.

ACCEPTED MANUSCRIPT

13. Zhao Q and Wagner HD. Two-dimensional strain mapping in model fiber-polymer composites using nanotube Raman sensing. Composite: Part A, 2003, 34, 1219 – 1225.

14. Zhao Q, Frogley MD, Wagner HD. The use of carbon nanotubes to sense matrix stresses around a single glass fiber. Compos. Sci. and Tech., 2001, 61, 2139 – 2143.

15. Sureeptanapas P and Young R.J. SWNT Composite Coatings as a Strain Sensor on Glass Fibres in Model Epoxy Composites, Compos. Sci. and Tech. 2009, **6,** 1547-1552.

16. Sureeyatanapas P, Hejda M, Eichhorn S.J. and Young R.J, Comparing Single-walled Carbon Nanotubes and Samarium Oxide as Strain Sensors for Model Glass-fibre / Epoxy Composites, Compos. Sci. and Tech., 2010, **70**, 88-93.

Figures Captions

Figure 1 Experimental arrangement for 6 image phase stepped Photoelasticity

Figure 2 The geometrical correction of the principal stress difference as a function of resin thickness (*t*)

Figure 3 Contour maps of fringe order in the matrix resin at the free-end of an E-glass fibre at 18.38 MPa

Figure 4 Contour maps of fringe order in the matrix resin at the free-end of an E-glass fibre at 25.61 MPa

Figure 5 Contour maps of fringe order in the matrix resin at the free-end of an E-glass fibre at 32.53 MPa

Figure 6 The profiles of interfacial shear stress determined by photoelastic analysis for E-glass fibre-end embedded in epoxy matrix at 18.38, 25.61 and 32.53 MPa

Figure 7 Contour maps of fringe order in matrix resin around the fibre-break of an E-glass fibre at 24.69 MPa

ACCEPTED MANUSCRIPT

Figure 8 Contour maps of fringe order in matrix resin around the fibre-break of an E-glass fibre at 33.09 MPa

Figure 9 The profiles of interfacial shear stress determined by photoelastic analysis at a fibre-break in an E-glass fibre embedded in epoxy matrix at 24.69 and 33.09 MPa

Figure 10 Micrograph showing interfacial debonding around a fibre-break under the optical microcope (POLYVAR) after loading axially to 33.09 MPa

Table 1 Properties of the E-glass fibre and the matrix resin

Matrix resin		E-glass fibres	
Young's modulus (GPa)	3.2 ± 0.4	Young's modulus(GPa)	72 ± 2.7
Tensile strength (MPa)	72 ± 3.5	Diameter (μm)	25 ± 1.2
Tensile yield stress	48 ± 2.3		
Shear yield stress (MPa)	27.7 ± 1.4		
Tensile yield strain (%)	1.5 ± 0.4		
Stress-fringe constant (MPa/fringe/mm)	20.23 ± 0.2		

ACCEPTED MANUSCRIPT

Table 2 Orientations of the polarizer (P), quarter wave plates (Q_1, Q_2) and analyzer (A)

Light intensity of each image	P	Q_1	Q_2 / α	A / β
i_1	0	-45°	0	45°
i_2			0	-45°
i_3			0	0
i_4			-45°	-45°
i_5			-90°	-90°
i_6			-135°	-135°

fig 1

ACCEPTED MANUSCRIPT

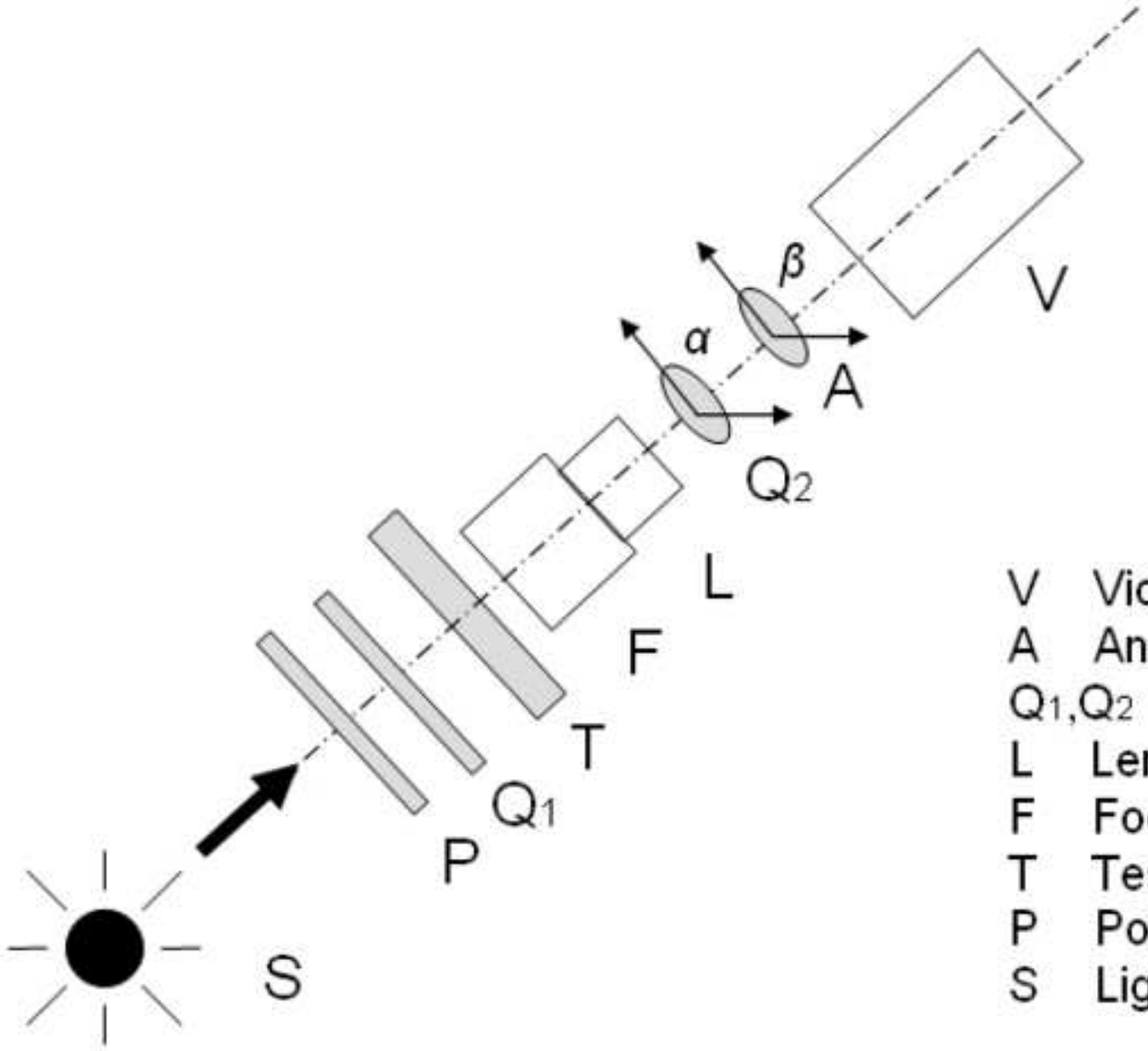

V Video camera
A Analyser
Q_1,Q_2 Quarter-wave plate
L Lens, objective
F Focal lens
T Test specimen
P Polariser
S Light source

Fig 2 revised

ACCEPTED MANUSCRIPT

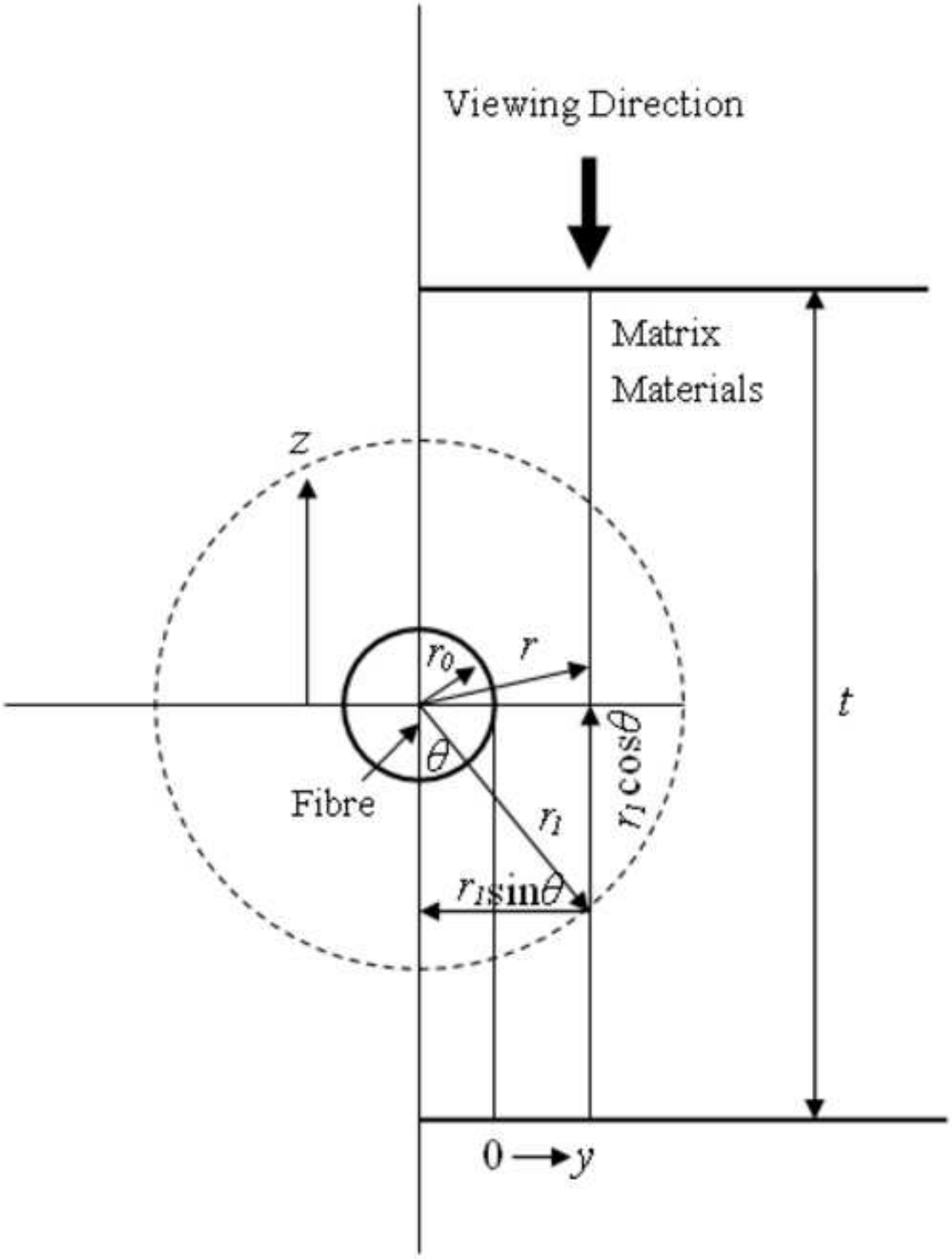

Fig 3

ACCEPTED MANUSCRIPT

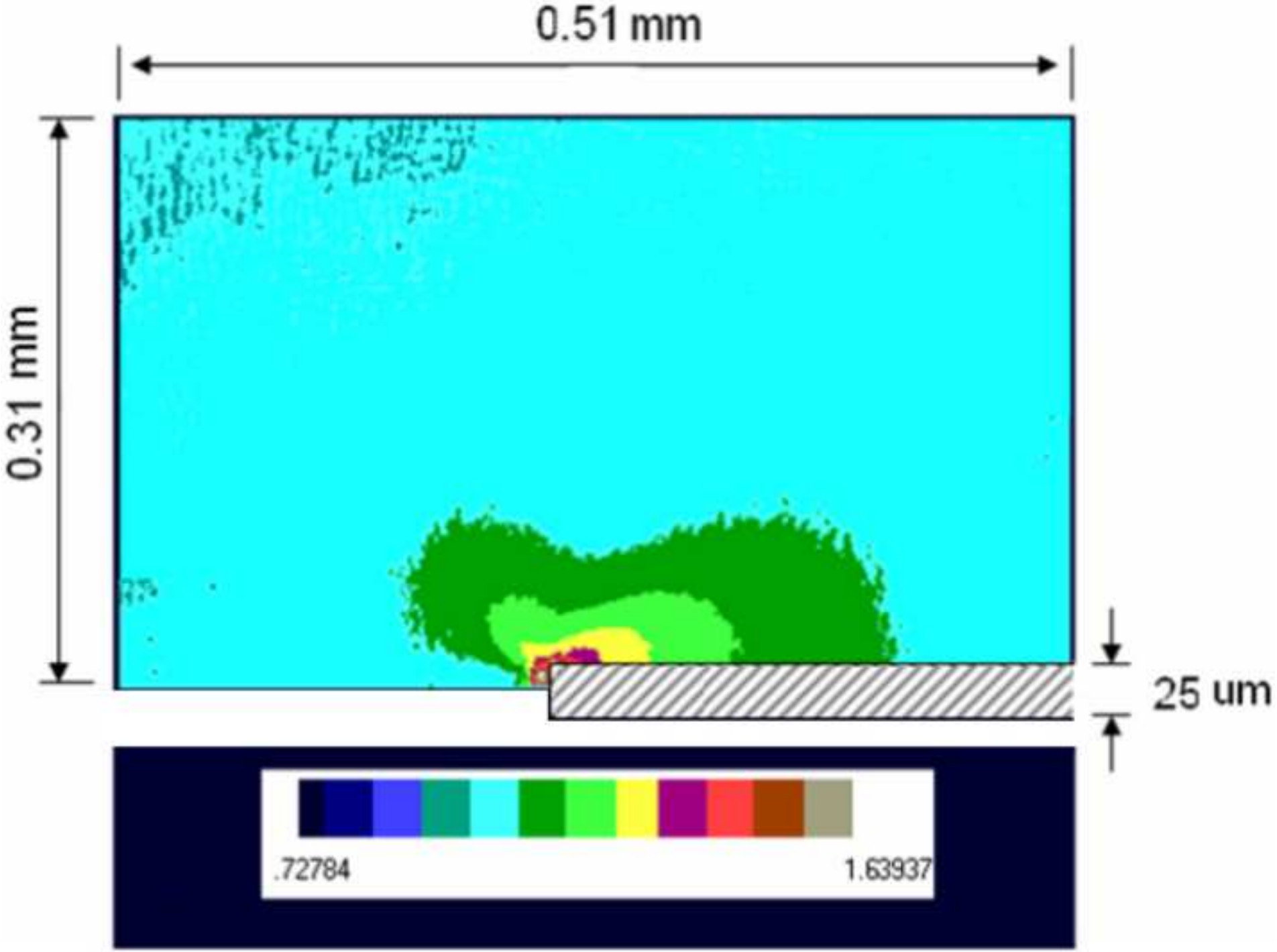

Fig4

ACCEPTED MANUSCRIPT

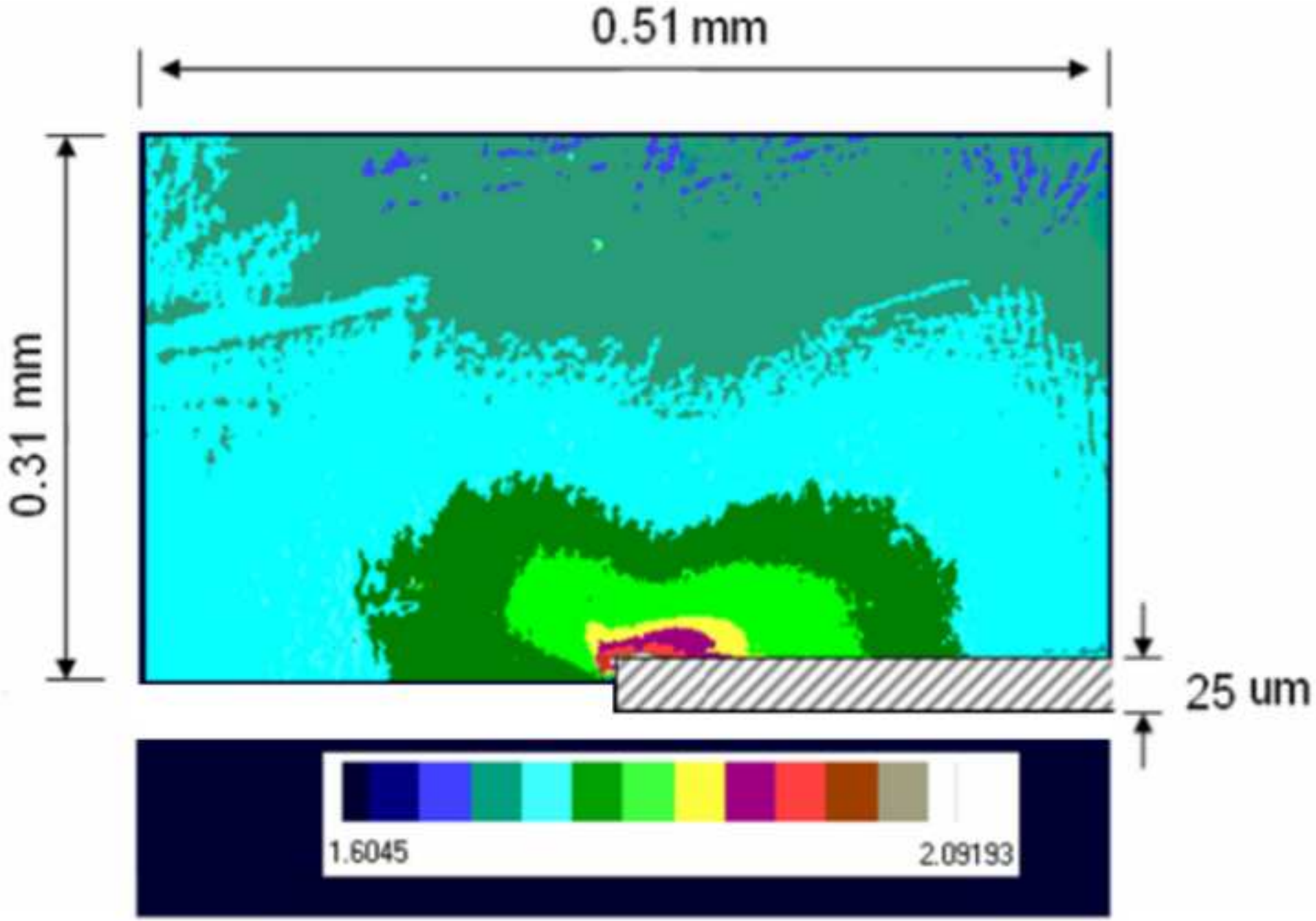

Fig5

ACCEPTED MANUSCRIPT

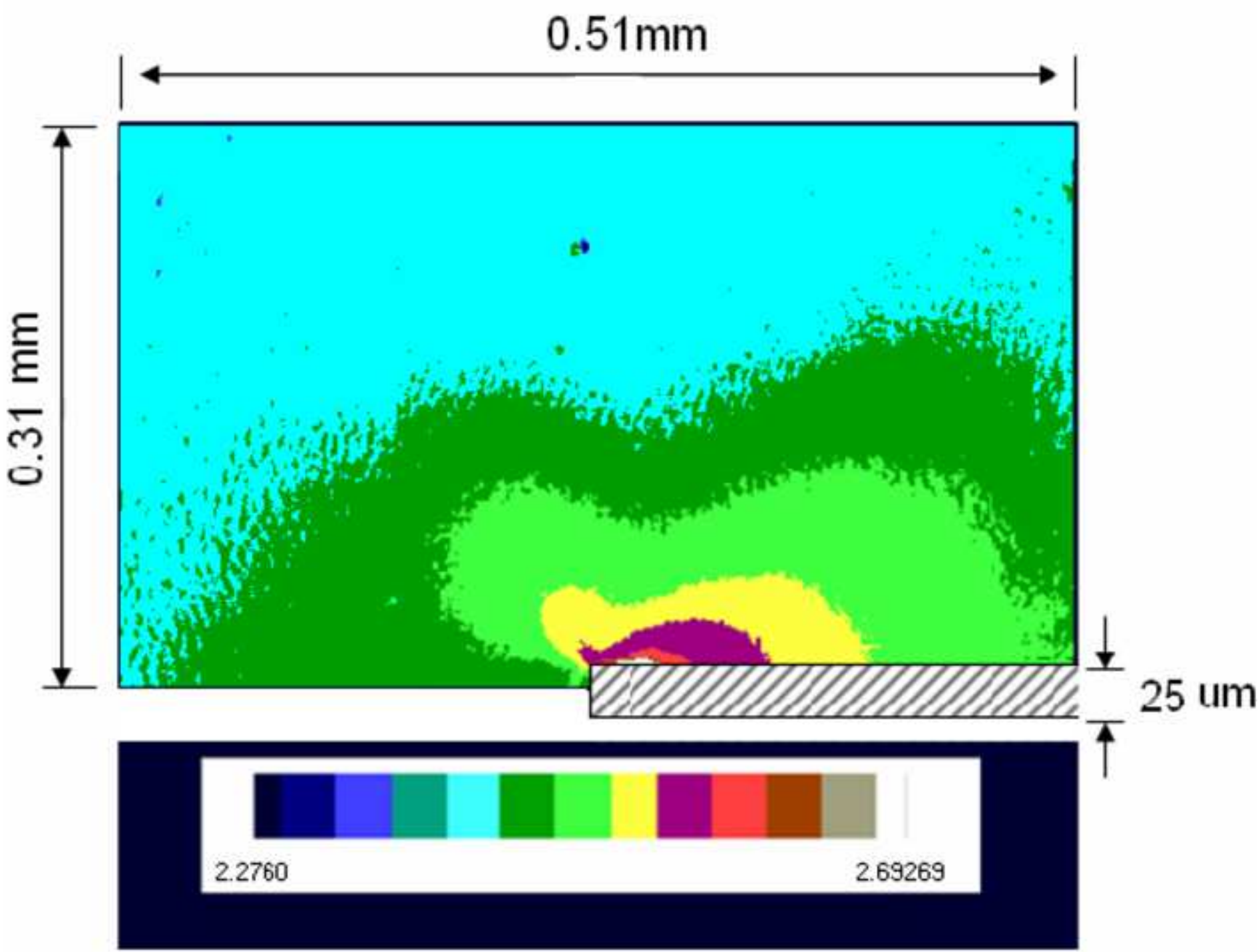

Figure 6

ACCEPTED MANUSCRIPT

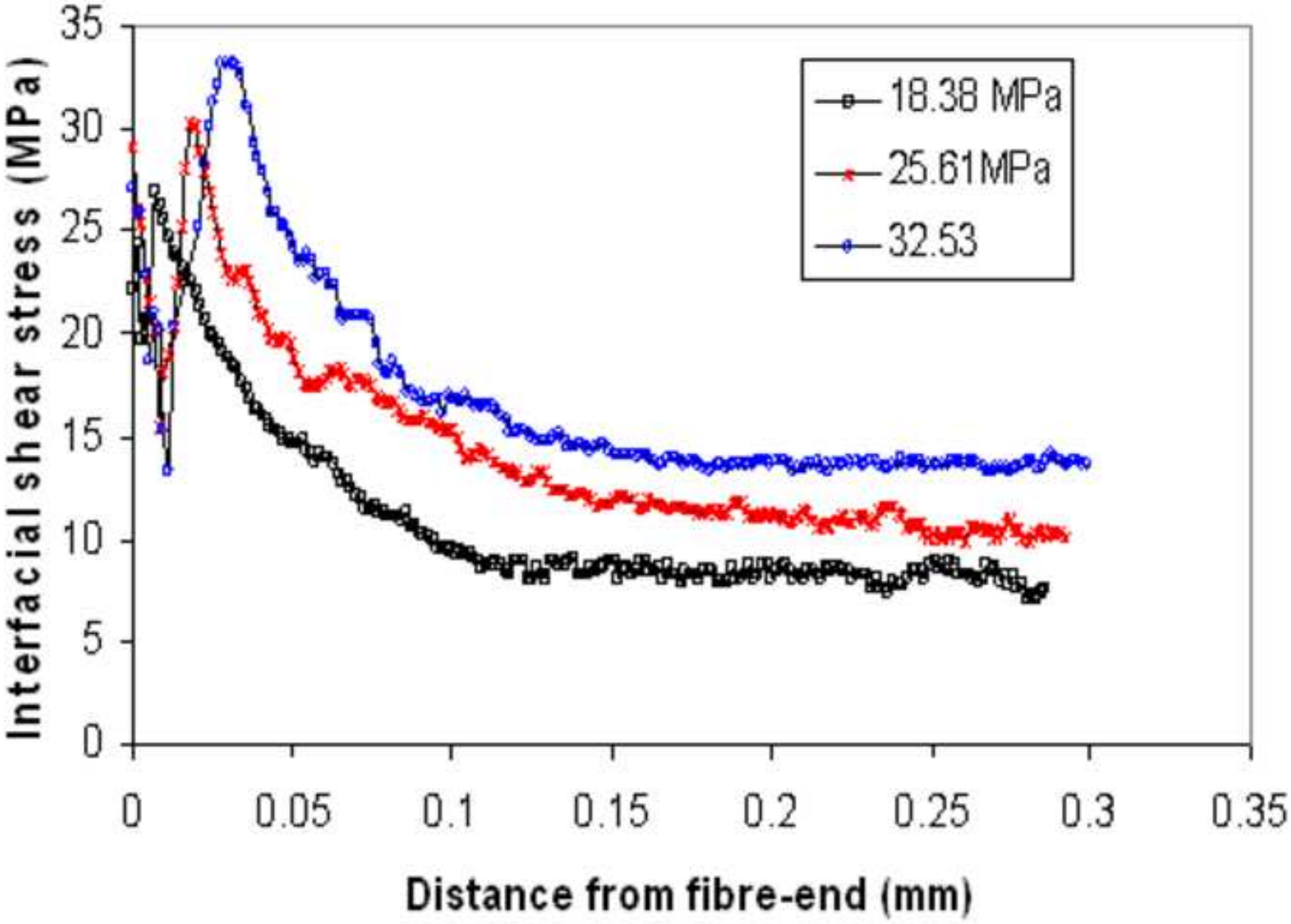

Fig7

ACCEPTED MANUSCRIPT

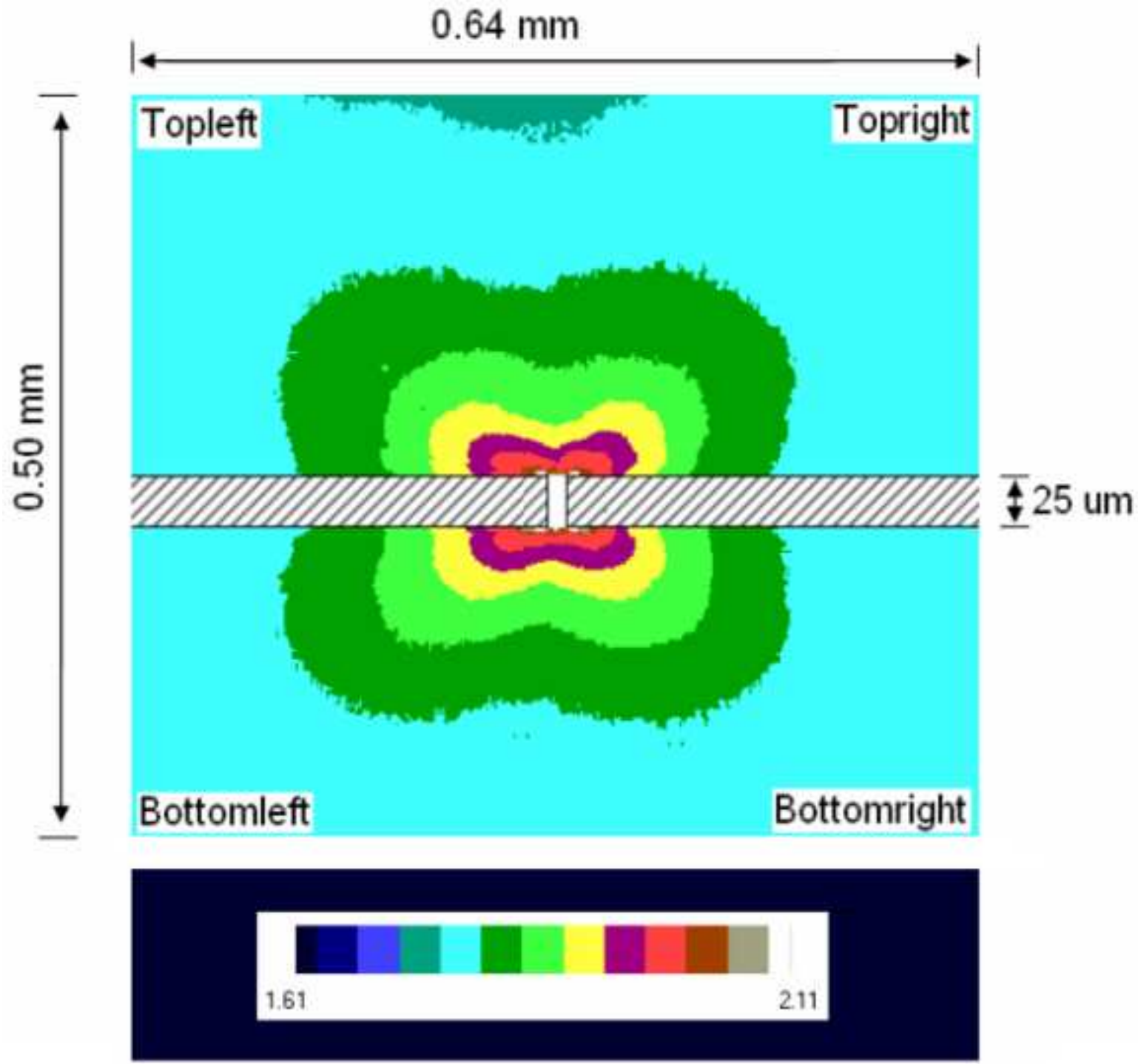

Fig8

ACCEPTED MANUSCRIPT

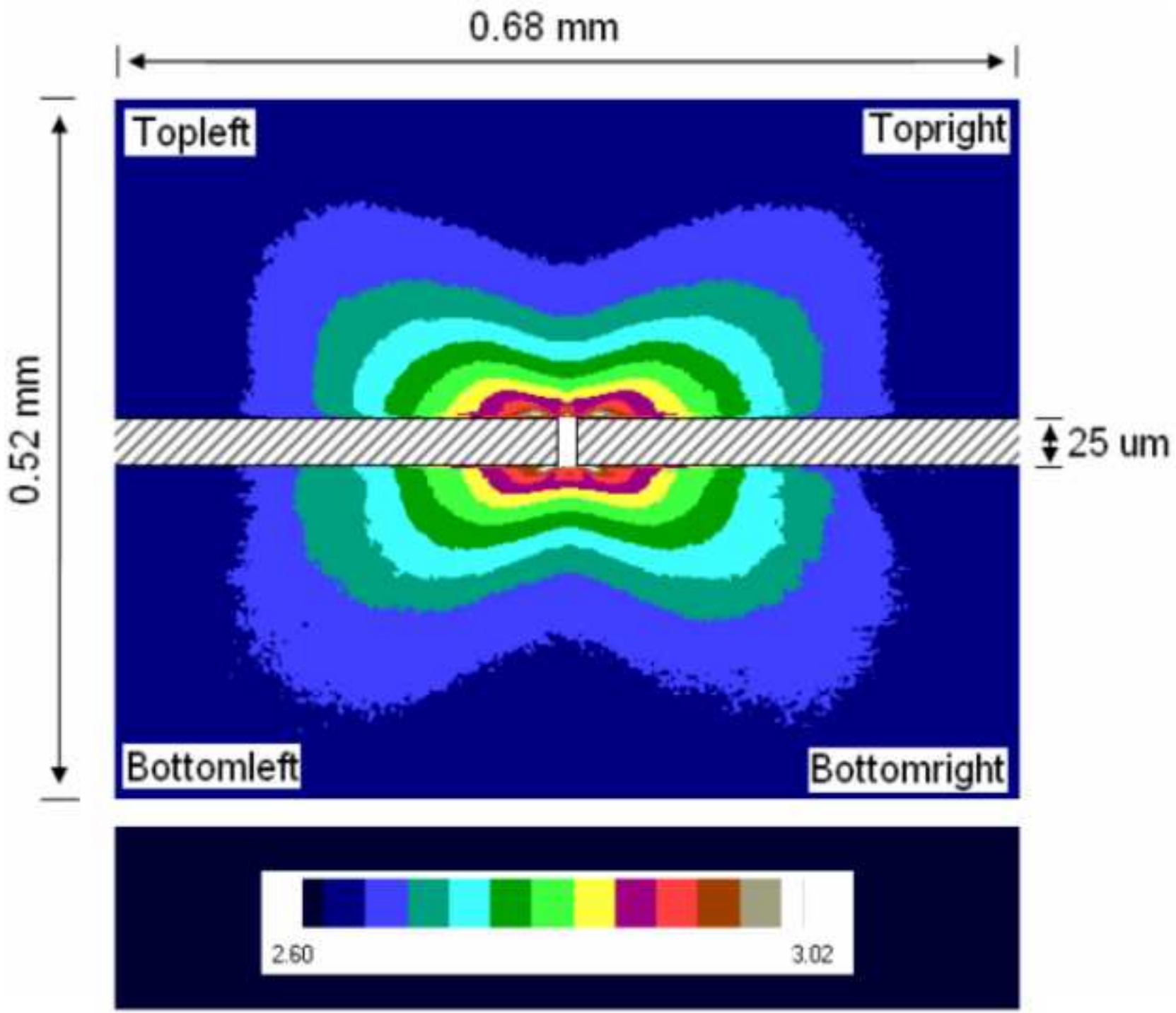

Fig9

ACCEPTED MANUSCRIPT

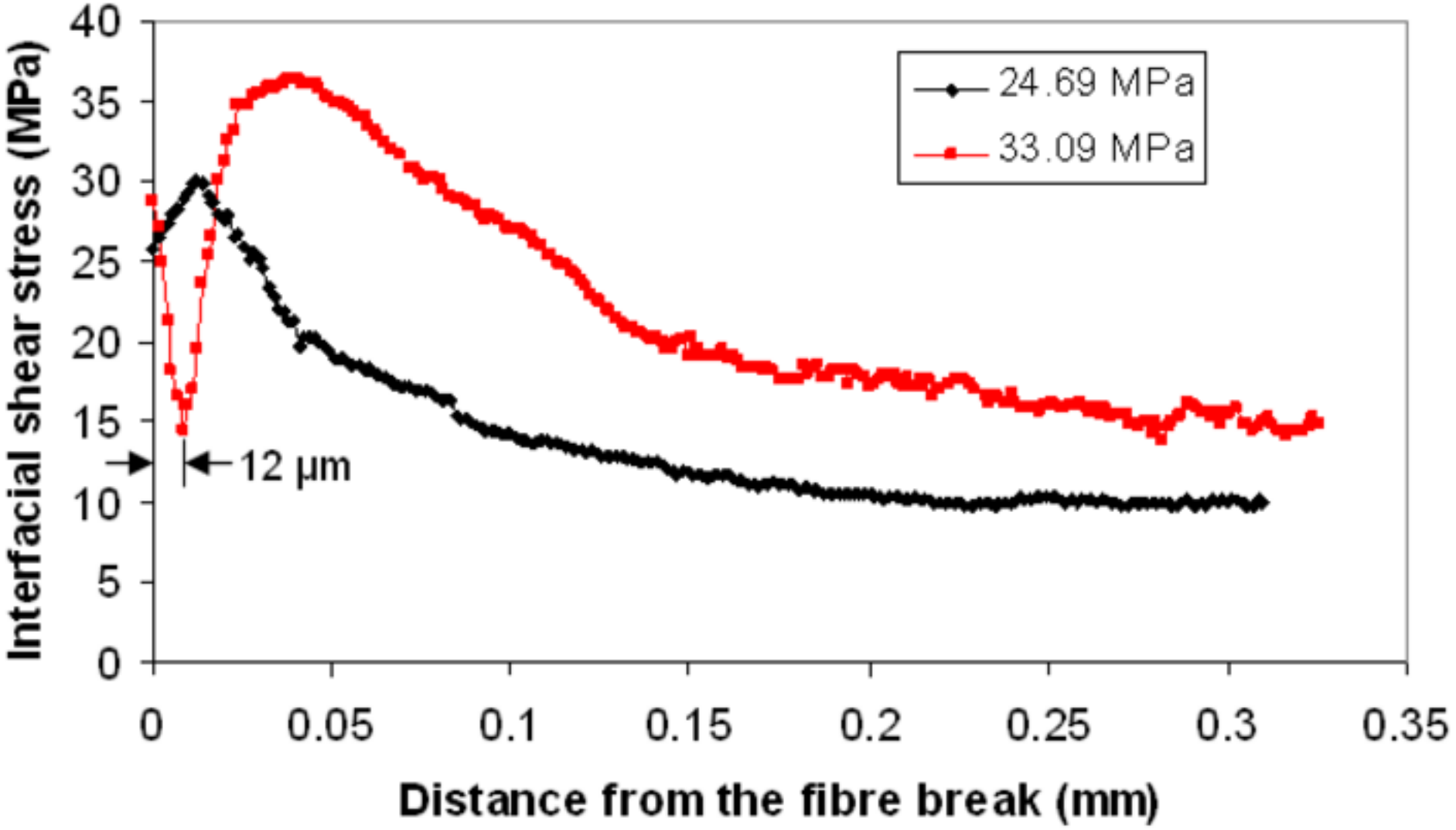

Fig10

ACCEPTED MANUSCRIPT